Electronic Supplementary Material (ESI) for Inorganic Chemistry Frontiers.

Supporting Information for

A Wheel-Shaped Gallium-Sulfide Molecular Ring with Enhanced Photocatalytic Activity via Indium Alloying

Tao Wu,*[,a,b] Bing Han,[b] Jia-Xin Liu,[a] Jiaxu Zhang,[b] Chaozhuang Xue,[b] Xiang Wang,*[,c] and Dong-Sheng Li[d]

[a] College of Chemistry and Materials Science, Guangdong Provincial Key Laboratory of Functional Supramolecular Coordination Materials and Applications, Jinan University, Guangzhou, Guangdong 510632, China.

[b] College of Chemistry, Chemical Engineering and Materials Science, Soochow University, Suzhou, Jiangsu 215123, China.

[c] School of New Energy Materials and Chemistry, Leshan Normal University, Leshan, Sichuan 614004, China.

[d] College of Materials and Chemical Engineering, Hubei Provincial Collaborative Innovation Center for New Energy Microgrid, Key Laboratory of Inorganic Nonmetallic Crystalline and Energy Conversion Materials, China Three Gorges University, Yichang, Hubei 443002, China

* Corresponding author E-mails: wutao@jnu.edu.cn; *516443537@qq.com.*

Experimental Section

Single-crystal X-ray diffraction (SCXRD). Single-crystal X-ray diffraction measurements were performed on a Bruker Photon II CPAD area diffractometer using graphite mono-chromated Mo-Kα (λ = 0.71073 Å) radiation at 120 K controlled by nitrogen-flow. The structure was solved by direct method using SHELXS-2014 and the refinement against all reflections of the compounds was performed using SHELXL-2014. The highly disordered solvent molecules were subtracted from the reflection data by using the SQUEEZE method in PLATON program. A summary of the structure refinement parameters is presented in Table S1.

Powder X-ray Diffraction (PXRD). PXRD data were recorded on a desktop diffractometer (D2 PHASER, Bruker, Germany) using Cu-Kα (λ = 1.54184 Å) radiation operated at 30 kV and 10 mA.

Elemental Analysis. Energy dispersive spectroscopy (EDS) analysis was performed on scanning electron microscope (SEM) equipped with energy dispersive spectroscopy detector. An accelerating voltage of 25 kV and 40 s accumulation time were applied. Elemental analysis (EA) of C, H, and N was performed on Vario EL III elemental analyzer. The elemental ratio of In/Ga was determined by using both an inductively coupled plasma atomic emission spectrometer 710-ES (ICP-AES, Varian Instruments): In/Ga=0.491.

Thermogravimetric Analysis (TGA). TGA measurement was performed with a Shimadzu TGA-50 system under nitrogen flow. The TG curve was performed by heating the sample from room temperature to 800 °C with heating rate of 10 °C /min.

Fourier Transform Infrared Absorption. Fourier transform-Infrared spectral analysis was performed on a Thermo Nicolet Avatar 6700 FT-IR spectrometer with cesium iodide optics allowing the instrument to observe from 600-4000 cm^{-1}.

UV-Vis Absorption. Room-temperature solid-state UV-Vis diffusion reflectance spectra of crystal samples were measured on a SHIMADZU UV-3600 UV-Vis-NIR spectrophotometer coupled with an integrating sphere by using $BaSO_4$ powder as the reflectance reference. The absorption spectra were calculated from reflectance spectra by using the Kubelka-Munk function: $F(R)=\alpha/S=(1-R)^2/2R$, where R, α, and S are the reflection, the absorption and the scattering coefficient, respectively. To determine the band edge of the direct-gap semiconductor, the relation between the absorption coefficients (α) and the incident photon energy ($h\upsilon$) is exhibited as $\alpha h\upsilon = A\times(h\upsilon - E_g)^{1/2}$, where A is a constant that relates to the effective masses associated with the valence and conduction bands, and E_g is the optical transition gap of the solid material. The band gap of the obtained samples can be determined from the Tauc plot with $[F(R)\times h\upsilon]^2$ vs. $h\upsilon$ by extrapolating the linear region to the abscissa.

Photoelectric Response. The photocurrent experiments were performed on a CHI760E electrochemistry workstation in standard three-electrode configuration, with the sample coated ITO glass (6×1 cm, effective area is around 1 cm^2) as the working electrode, a Pt wire as the auxiliary electrode, and a saturated calomel electrode (SCE) as the reference electrode. The light source is a 150 W high-pressure xenon lamp, located 19 cm away from the surface of the ITO electrode and the illumination intensity on the surface of the photoelectrode was ~100 mW/cm^2. Sodium sulfate aqueous solution (0.5 M, 100 mL) was used as the supporting electrolyte. Typical preparation of the working electrode is as follows: 5.0 mg of ground sample powder was dispersed in 10 mL isopropanol with the presence of 1.0 mg of $Mg(NO_3)_2\cdot 6H_2O$ (addition $Mg(NO_3)_2\cdot 6H_2O$ for increasing conductivity). The sealed mixture suspension was continuously stirred for one day, and then ultrasonicated for half hour before electrophoretic deposition. The clean and sleek Pt plate electrode was used as anode, and the clean indium-tin-oxide (ITO) conductive glass as cathode. The whole electro-deposition process lasted for 30 minutes under a constant working voltage of 30 V. The obtained ITO electrode decorated with **WSC-1** or

WSC-1-In film on its surface was finally washed with ethanol to remove residual isopropanol and $Mg(NO_3)_2$ salt.

Electrochemical Mott-Schottky Experiments. Mott-Schottky plots were measured by conducting impedance-frequency measurement. The capacitance of the semiconductor-electrolyte interface was collected at different frequency of 1000, 1500 and 2000 Hz. Before testing, 2 mg finely ground sample was placed in a sample tube and then 420 μL ethanol, 30 μL water and 50 μL D-521 Nafion solution (5 *wt*% in propanol) were mixed and then ultrasonicated for 1 h. The mixed sample (40 μL) was deposited on a 6×1 cm^2 ITO conductive glass with a sample deposition area of 1×1 cm^2 and then dried at room temperature. Finally, electrochemical experiments were carried out in a same three-electrode system as for photocurrent measurement with sample coated ITO glass as the working electrode, a Pt wire as the auxiliary electrode, a Ag/AgCl electrode as the reference electrode and 0.5 M sodium sulfate solution as the electrolyte.

Photocatalytic Hydrogen Generation: The H_2 production experiment were carried out in a closed vacuum glass gas-circulation system with a top window (Perfect-Light, Labsolar-6A). Firstly, 25 mg samples were finely ground and mixed with 90 mL deionized H_2O and 10 mL triethanolamine as the sacrificial reagent. The mixture was then poured into a 250 mL quartz vessel, where 1 mg (equal to 2 *wt.*% Pt) $Pt(NH_3)_4(NO_3)_2$ was added. Next, this system was evacuated to *ca.* 1.0 kPa at low temperature (5 ºC) and then irradiated by a 300 W Xe lamp. During the photocatalytic reaction, the reaction solution was under a continuous magnetic stirring at 5 ºC by a flow of cooling water. Finally, the evolved H_2 was analyzed by gas chromatography equipped with a thermal conductive detector (GC9790II, Fuli) and N_2 as carrier gas.

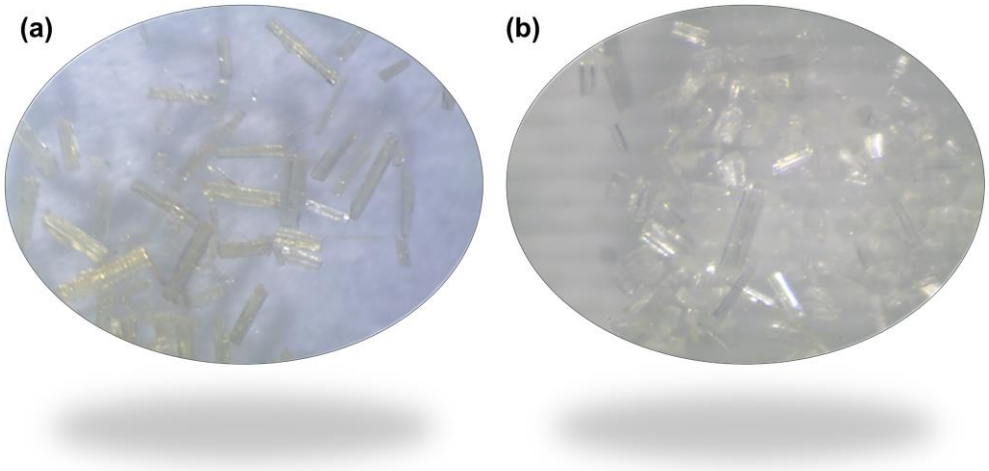

Figure S1. Photographs of the crystals of (a) **WSC-1** and (b) **WSC-1-In**.

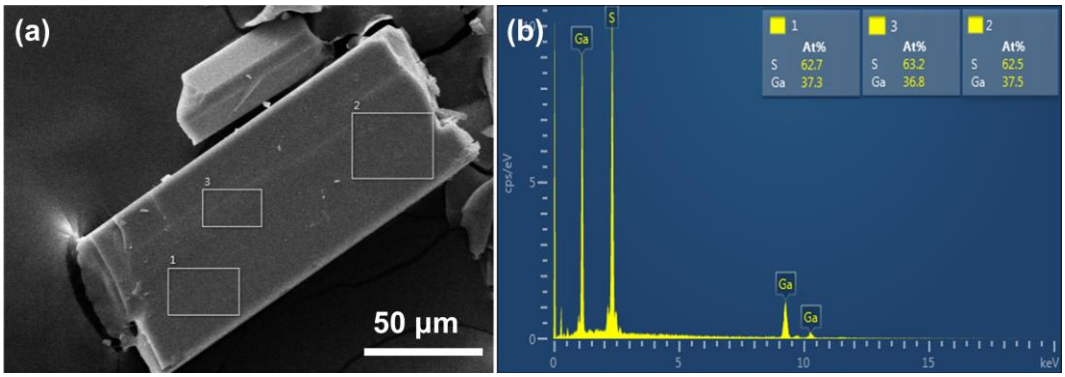

Figure S2. (a) SEM images of as-synthesized **WSC-1** crystal and (b) corresponding energy dispersive spectroscopy (EDS) of **WSC-1**.

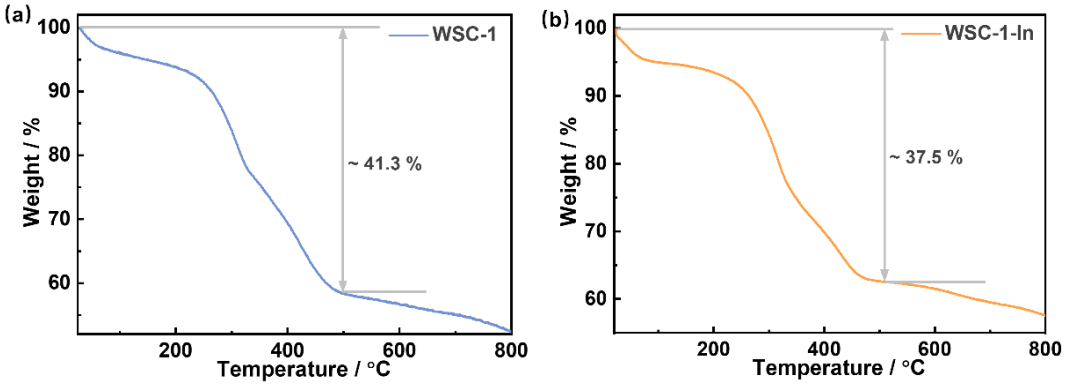

Figure S3. TGA curves of (a) **WSC-1** and (b) **WSC-1-In**.

The thermogravimetric (TG) analysis of **WCS-1** (Figure S3a) showed multiple decomposition steps from room temperature to *ca.* 500 °C under N_2 conditions,

indicating the loss of non-coordinated and coordinated cyclopentylamine molecules in **WSC-1**. And the total loss (~ 41.3%) is consistent with weight ratio of cyclopentylamine molecules (41.0 %) in the empirical formula of **WSC-1** ($[Ga_{24}S_{40}(C_5H_{11}N)_{16}(C_5H_{12}N)_8]$). As for **WSC-1-In** (Figure S3b), similar process also occurred during the TG measurement and the total loss (~ 37.5 %) is consistent with weight ratio of cyclopentylamine molecules (38.2 %) in the empirical formula of **WSC-1-In** ($[Ga_{16}In_8S_{40}(C_5H_{11}N)_{16}(C_5H_{12}N)_8]$).

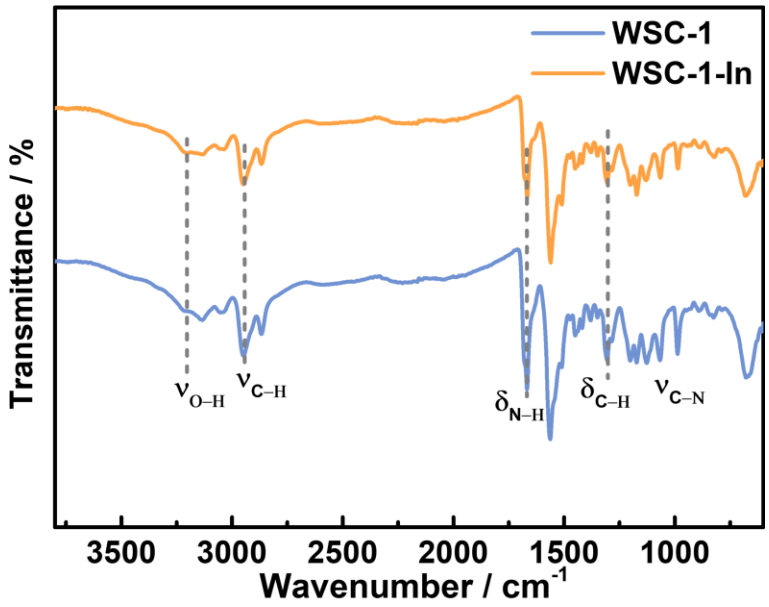

Figure S4. FTIR spectrum of (a) **WSC-1** (b) **WSC-1-In**.

The broad vibrational bands of IR at about 3440 and 3250 cm^{-1} indicate the presence of the $-NH_2$ group and H_2O molecules. Those at about 2920 and 2840 cm^{-1} are assigned to the C−H vibrational bands of CPA molecules.

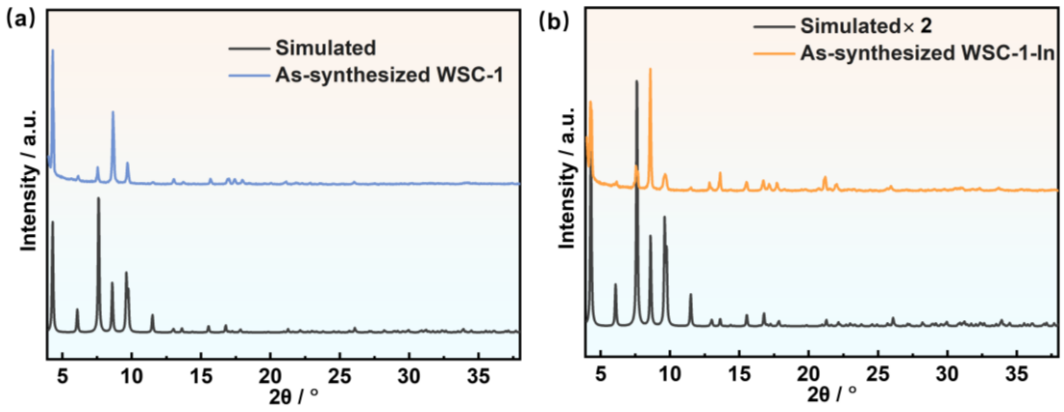

Figure S5. The simulated and experimental PXRD patterns of as-synthesized **WSC-1** and **WSC-1-In**.

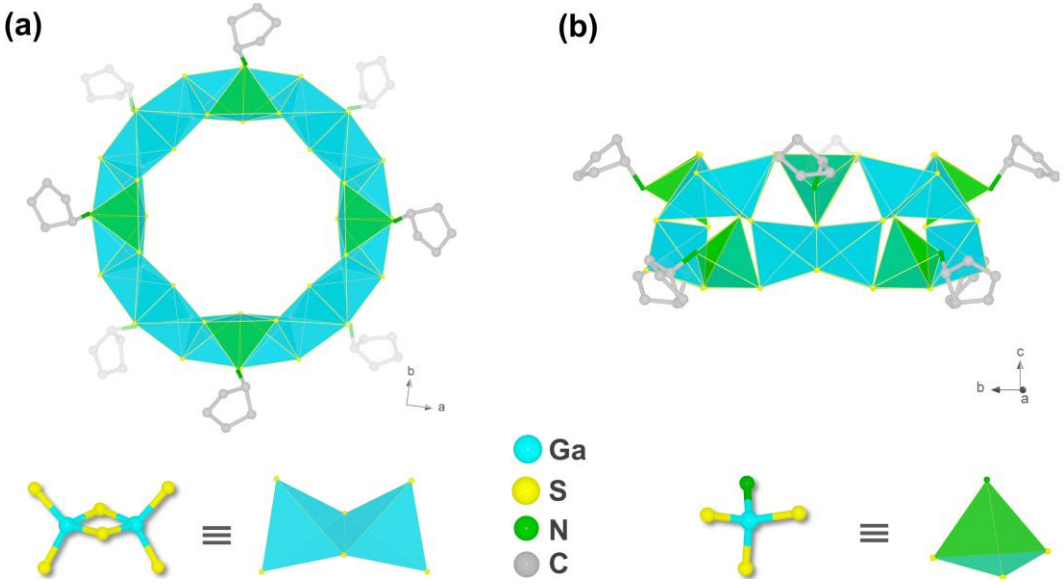

Figure S6. (a) Top down and (b) side view of the polyhedral model of wheel-shaped **WSC-1** molecular ring. Hydrogen atoms are omitted for clarity.

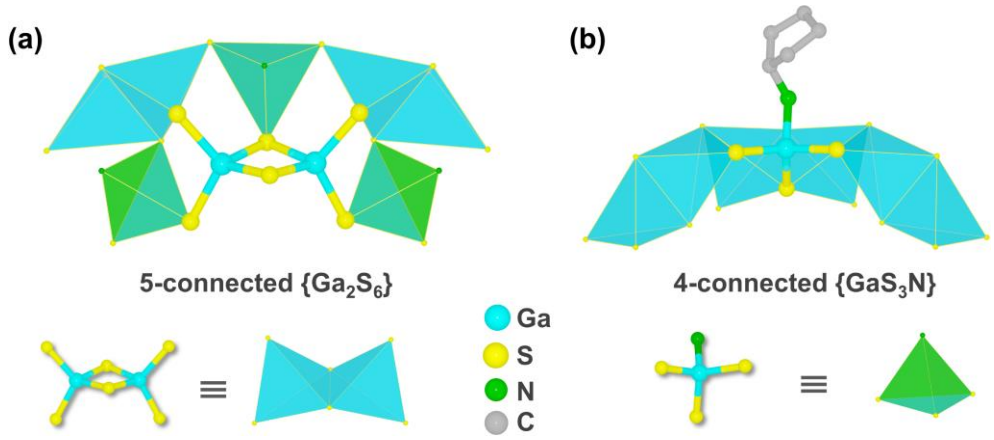

Figure S7. View of the polyhedral/ball-and-stick models of (a) 5-connected $\{Ga_2S_6\}$ and (b) 4-connected $\{GaS_3N\}$ unit. Hydrogen atoms are omitted for clarity.

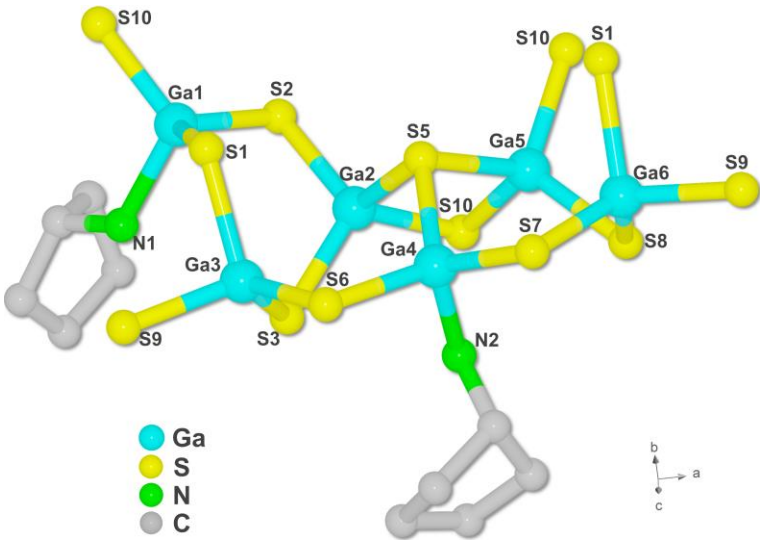

Figure S8. The asymmetric unit of **WSC-1** with the selected labeling scheme. Hydrogen atoms are omitted for clarity.

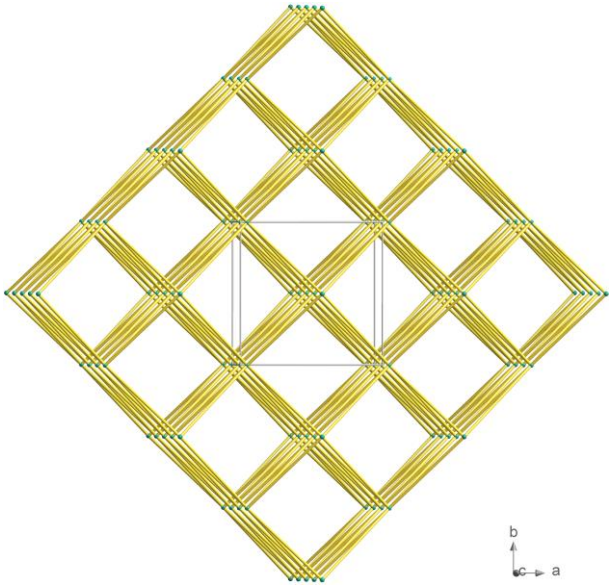

Figure S9. Illustration of the squashed *BCU*-type arrangement mode of ring clusters in **WSC-1** *via* connecting the centers of adjacent cluster (viewed along *c* axis).

By treating each barycenter of ring cluster as a pseudo atom (X) and connecting adjacent X atom (the X-X distance is ca. 21.4 Å), the arrangement mode of the **WSC-1** clusters is found to be squashed *BCU* (body centered cubic)-type superlattice.

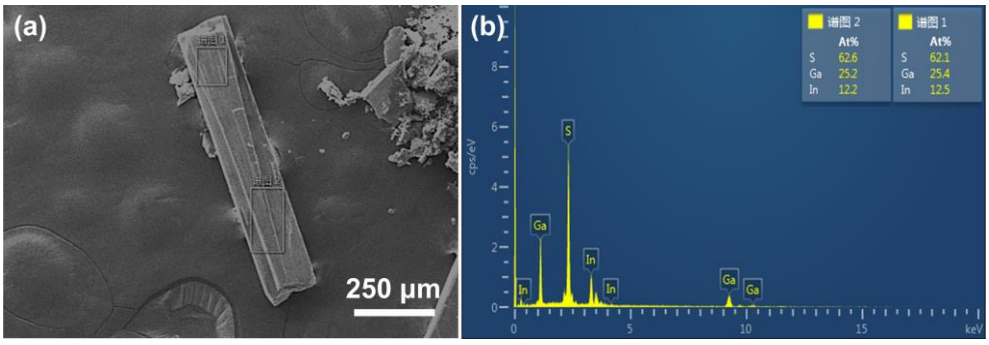

Figure S10. (a) SEM images of as-synthesized **WSC-1-In** crystal and (b) corresponding energy dispersive spectroscopy (EDS) of **WSC-1-In**.

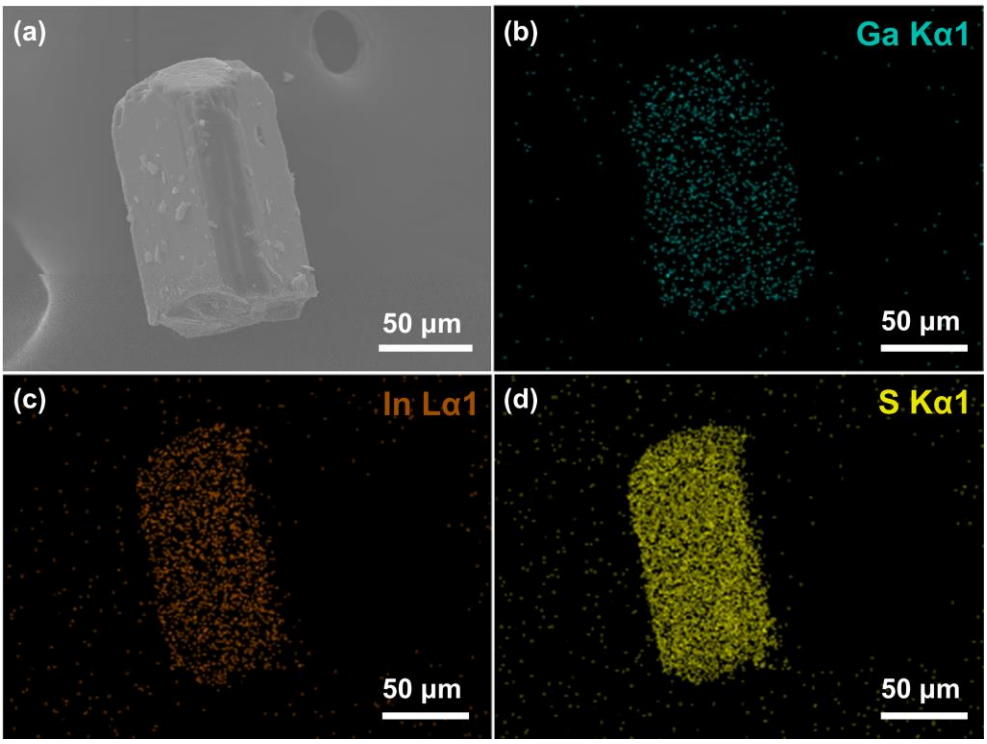

Figure S11. (a) SEM images and (b-d) corresponding elemental distribution maps of as-synthesized **WSC-1-In** crystal.

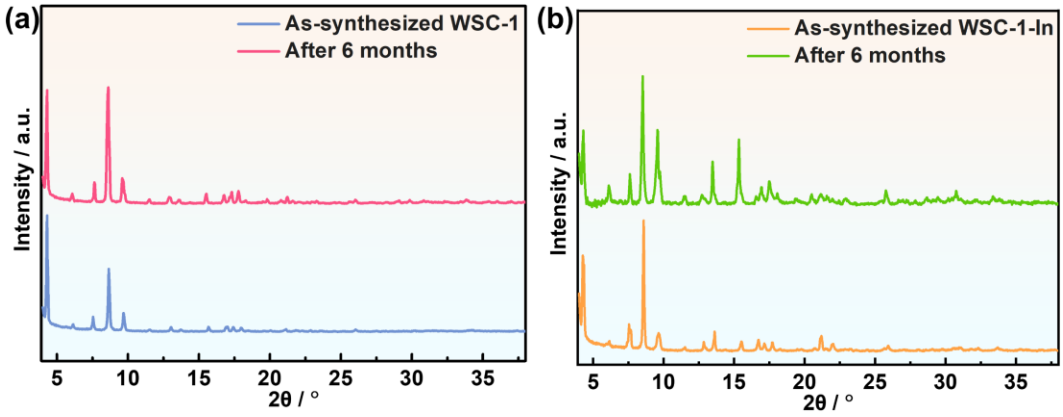

Figure S12. PXRD patterns of as-synthesized (a) **WSC-1** and (b) **WSC-1-In** exposed in air after six months.

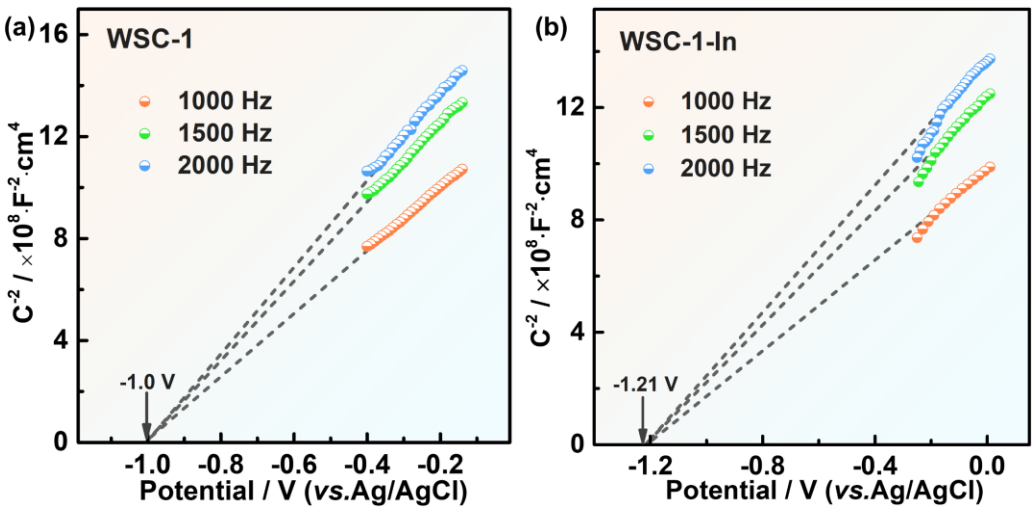

Figure S13. Mott-Schottky plots of (a) **WSC-1** and (b) **WSC-1-In** measured at different frequency.

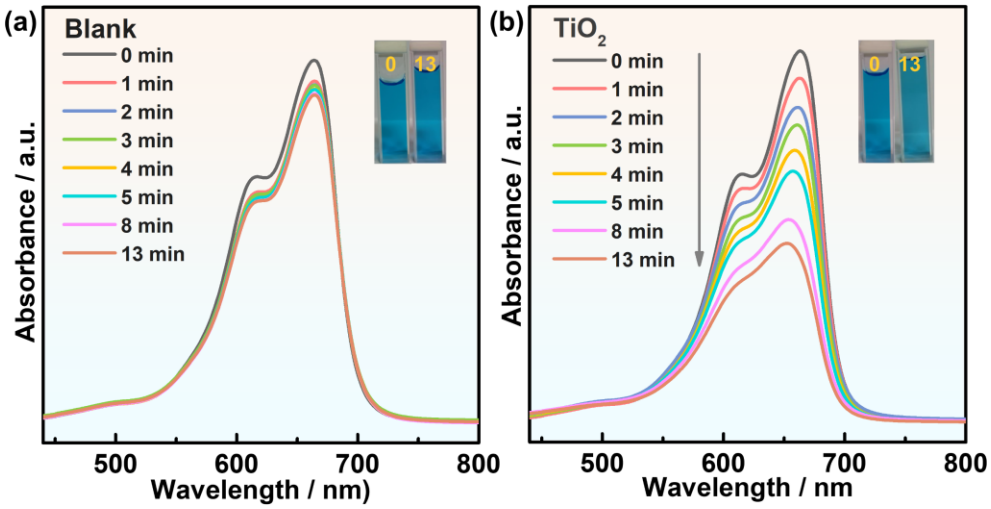

Figure S14. UV-Vis absorption spectra of MB versus time with (a) blank control and (b) TiO_2 as catalyst under full spectrum solar light irradiation. (Inset, photographs of MB solution before and after photodegradation).

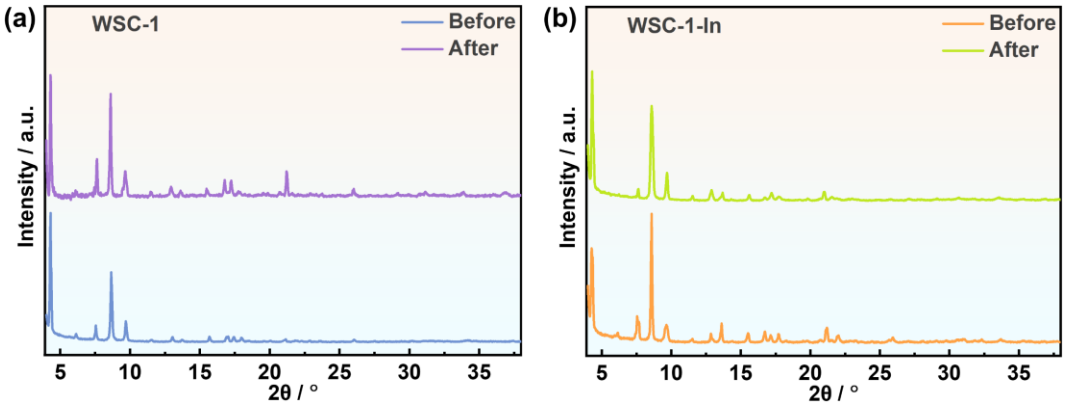

Figure S15. PXRD patterns of as-synthesized (a) **WSC-1** and (b) **WSC-1-In** before and after photocatalytic experiment.

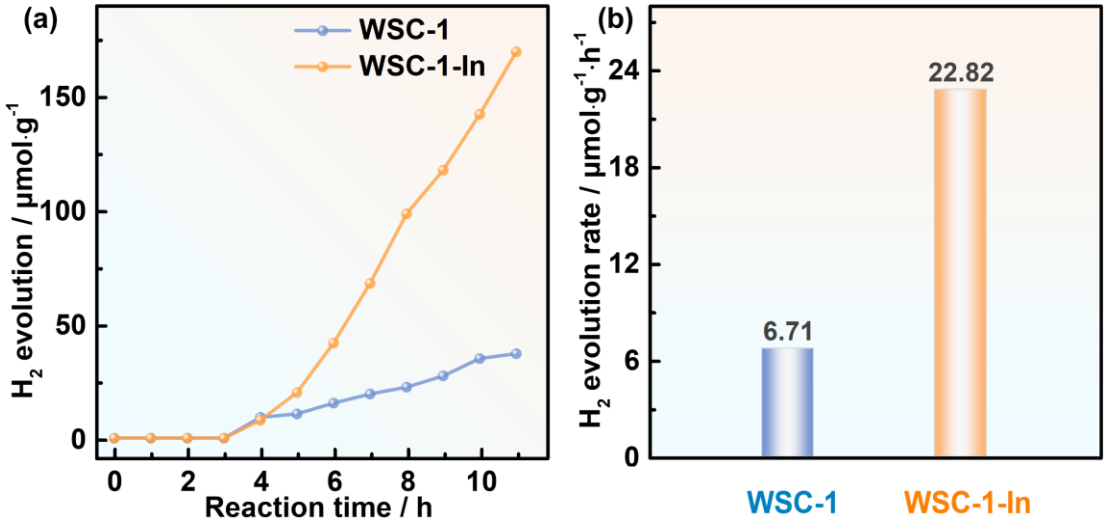

Figure S16. Comparison of the photocatalytic H_2 production of **WSC-1** and **WSC-1-In** under full spectrum solar light irradiation.

As the CBs of both title compounds are more negative than E_{H^+/H_2} (-0.41 V, pH=7), photocatalytic H_2 evolution was further investigated to assess the solar energy utilization of the title compounds.[1, 2] As shown in Figure S16a, the initial low H_2 generation rate could be attributed to the competition for electrons between Pt^{4+} species reduction and H^+ reduction in the initial 3h according to the literature.[1, 2] With continuous reduction of

$[Pt(NH_3)_4]^{2+}$ to Pt and the completion of reduction, more photoelectrons were used for H^+ reduction to H_2, resulting in a following gradual increased and finally stable H_2 evolution rate.[1, 2] And the possible mechanism for the photocatalytic H_2 evolution is proposed as follows.[1, 2] Upon solar light absorption, photo-generated electrons are excited from VB to CB and then transferred and trapped by Pt which generated from photoreduction of $[Pt(NH_3)_4]^{2+}$. The as-formed Pt acted as a co-catalyst for accepting photoelectron to reduce surface-adsorbed H^+ to H_2. Meanwhile, the TEOA molecules acting as a hole scavenger are oxidized to carbonaceous materials by the photogenerated holes in the VB. As the CB of **WSC-1-In** is more negative than that of **WSC-1** (Figure S19), a stronger driving force for H^+ reduction is afforded by WSC-1-In, resulting larger H_2 generation rate for **WSC-1-In**.[1, 2]

Table S1. Crystallographic data and structure refinement parameters of **WSC-1** (As the diffraction capability of cluster-based chalcogenide is usually weak, especially for the structures that are constructed by isolated clusters,[3] the crystal data for **WSC-1-In** is not available due to its poor diffraction data).

Compound	**WSC-1**
Empirical formula	$C_{40}H_{88}Ga_{24}N_8S_{40}$
Formula weight	3637.13
Crystal morphology	prism
Crystal system	Tetragonal
Space group	*I4*
Z	2
T/K	119.99
λ/Å	0.71073
a/Å	28.870(2)
b/Å	28.870(2)
c/Å	12.6517(9)
α/°	90
β/°	90
γ/°	90
V/Å^3	10545.0(16)
D (g/cm^3)	1.140
μ/mm^{-1}	3.420
F(000)	3500.0
Collected reflections	44737
Independent reflections	9636
GOF on F^2	0.987
R_1, wR_2 ($I>2\sigma(I)$)	0.0467, 0.1301
R_1, wR_2 (all data)	0.0934, 0.1623

Table S2. Selected important bond lengths for **WSC-1**.

Bond	Length/Å
Ga1−S2	2.236(4)
Ga1−S1	2.270(4)
Ga1−S10	2.206(5)
Ga1−N1	2.053(12)
Ga2−S3	2.277(4)
Ga2−S4	2.268(5)
Ga2−S2	2.254(4)
Ga2−S5	2.350(4)
Ga3−S3	2.278(4)
Ga3−S6	2.220(4)
Ga3−S9	2.229(4)
Ga3−S1	2.358(4)
Ga4−S6	2.238(4)
Ga4−S7	2.203(4)
Ga4−S5	2.324(4)
Ga4−N2[a]	1.98(4)
Ga5−S4	2.255(5)
Ga5−S8	2.268(5)
Ga5−S5	2.371(5)
Ga5−S10	2.258(5)
Ga6−S9	2.257(4)
Ga6−S8	2.267(5)
Ga6−S7	2.219(4)
Ga6−S1	2.378(5)

[a] $d_{Ga4\text{-}N2} = (d_{Ga4\text{-}N2}+d_{Ga4\text{-}N2A})/2$,

Table S3. Selected important bond angles for **WSC-1**.

Bond	Angle/°	Bond	Angle/°
S2−Ga1−S1	114.48(17)	S4−Ga5−S5	95.45(16)
S10−Ga1−S2	110.74(18)	S4−Ga5−S10	112.04(17)
S10−Ga1−S1	113.42(17)	S8−Ga5−S5	112.25(14)
N1−Ga1−S2	104.5(3)	S10−Ga5−S8	113.24(18)
N1−Ga1−S1	102.3(3)	S10−Ga5−S5	109.3(2)
N1−Ga1−S10	110.7(4)	S9−Ga6−S8	111.34(19)
S3−Ga2−S5	111.12(14)	S9−Ga6−S1	94.72(15)
S4−Ga2−S3	113.6(2)	S8−Ga6−S1	111.39(15)
S4−Ga2−S5	95.67(17)	S7−Ga6−S9	115.27(16)
S2−Ga2−S3	112.52(16)	S7−Ga6−S8	114.23(18)
S2−Ga2−S4	112.01(17)	S7−Ga6−S1	108.2(2)
S2−Ga2−S5	110.80(19)	Ga1−S2−Ga2	99.24(13)
S3−Ga3−S1	110.94(14)	Ga1−S1−Ga3	103.49(17)
S6−Ga3−S3	113.03(17)	Ga1−S1−Ga6	103.5(2)
S6−Ga3−S9	112.91(15)	Ga1−S10−Ga5	100.37(15)
S6−Ga3−S1	110.02(19)	Ga2−S3−Ga3	99.39(18)
S9−Ga3−S3	112.67(18)	Ga2−S5−Ga5	81.77(14)
S9−Ga3−S1	96.04(16)	Ga3−S6−Ga4	100.01(13)
S6−Ga4−S5	113.90(17)	Ga3−S1−Ga6	80.79(13)
S7−Ga4−S6	112.95(16)	Ga3−S9−Ga6	86.34(15)
S7−Ga4−S5	112.05(18)	Ga4−S7−Ga6	101.65(15)
N2−Ga4−S6[a]	105.55(15)	Ga4−S5−Ga2	103.6(2)
N2−Ga4−S7[a]	108.95(12)	Ga4−S5−Ga5	102.8(2)
N2−Ga4−S5[a]	102.55(10)	Ga5−S4−Ga2	86.18(18)
S4−Ga5−S8	113.3(2)	Ga6−S8−Ga5	98.7(2)

[a] $\theta_{N2-Ga4-Sx} = (\theta_{N2-Ga4-Sx} + \theta_{N2A-Ga4-Sx})/2$.

Table S4. Comparison of the main-group metal chalcogenides ring clusters and sulfides-based inorganic nanoring clusters.

Formula of anion cluster [a]	Metal		Chalcogenide	Cluster shape	Cluster size (Å) [c]	Ref.
	Type [b]	Number				
$[Ga_{24}S_{40}(CPA)_8]^{8-}$	**Ga**	**24**	**S**	**Wheel ring**	**ID: 9.92 OD: 15.72**	**This work**
$[Ge_{16}Se_{36}]^{8-}$	Ge	16	Se	Square ring	Inner size: 3.59×3.59 Outer size: 7.52×14.59	*JACS Au,* **2022**, *2*, 204
$[In_{18}Te_{30}(dach)_6]^{6-}$	In	18	Te	Wheel ring	ID: 8.25 OD: 15.54	*Inorg. Chem.,* **2012**, *51*, 1219
$[Mn_9In_{33}Se_{60}(dach)_{24}]^{3-}$	In	33	Se	Triangular ring	ID: 12.71 OD: 25.46	*Chem.Commun* **2015**,*51*,10668
$[Sb_3S_6]^{3-}$	Sb	3	S	Twisted triangular ring	ID: 2.96 OD: 3.98	*Cryst.Growth Des.* **2011**, *11*, 5554
$[Sb_6S_{12}]^{6-}$	Sb	6	S	Twisted starlike ring	ID: 5.08 OD: 10.56	
$[Na_2Fe_{18}S_{30}]^{8-}$	Fe	18	S	Ellipse ring	Inner size: 4.09×8.92 Outer size: 13.32×15.97	*J.Am.Chem.Soc.* **1988**, *110*, 6591
$[\beta-Na_2Fe_{18}S_{30}]^{8-}$	Fe	18	S	Ellipse ring	Inner size: 4.08×7.18 Outer size: 12.39×16.29	*J.Am.Chem.Soc.* **1992**, *114*, 2697

[a] The formula of cations and solvent molecules are omitted for simplicity. The abbreviations of organic molecules including the formulas are listed as follows: CPA — cyclopentylamine; dach — 1,2-diaminocyclohexane.

[b] The metallic element referred to metals participated in the linkage of ring cluster.

[c] For circular-like ring cluster, ID is the abbreviation of Inner diameter and OD means outer diameter. While for ellipse ring, the inner and outer size of cluster mean the length of short axis × length of long axis.

Table S5. Comparison of the solvent-accessible void space between several recent reported typical discrete cluster-based crystalline metal chalcogenides.

Formula of anion cluster [a]	Cluster type [b]	Intercluster packing pattern [c]	Solvent-accessible void space (%) [d]	Dispersion solvent	Ref.
$[Ga_{24}S_{40}(CPA)_8]^{8-}$	**Wheel-shaped ring**	**Elongated *BCU***	**56.0**	**Formamide**	**This work**
$[In_{18}Te_{30}(dach)_6]^{6-}$	Wheel-shaped ring	Squashed *BCU*	40.8	NA [e]	*Inorg. Chem.*, **2012**, *51*, 1219
$[Mn_9In_{33}Se_{60}(dach)_{24}]^{3-}{}_2$ $[In_{18}Se_{30}(dach)_6]^{6-}$	Triangular and wheel-shaped ring	3-fold interpenetrating twisted *PCU* [f]	49.5	Dach	*Chem.Commun.*, **2015**,*51*, 10668
$[Ge_4S_{10}]^{4-}$	T2	Elongated *BCU*	65.9	Water	*Inorg. Chem.*, **2017**, *56*, 3119
$[In_{10}S_{16}(DBN)_4]^{4-}$ (ISC-3)	T3	Twisted Cubic *Dia*	40.1	DMF	*J. Am. Chem. Soc.* **2012**, *134*, 3619
$[Sn_{10}O_8S_{16}]^{4-}$	T3	*MTN*	77.2	Water	*Chem.Commun.*, **2020**,*56*,8388.
$[Zn_4Ga_{14}Sn_2S_{35}]^{12-}$ (OCF-40-ZnGaSnS)	T4	*BCU*	59.4	DMF/DMSO/Piperidine	*J. Am. Chem. Soc.* **2010**, *132*, 10823
$[Cd_4In_{16}S_{31}(DBN)_4]^{6-}$ (ISC-5)	T4	Cubic *Dia*	59	DMSO	*J. Am. Chem. Soc.* **2012**, *134*, 3619
$[Cd_3In_{17}S_{13}Se_{18}Cl_4]^{9-}$	T4	Twisted Cubic *Dia*	63.5	DMSO	*Inorg. Chem.* **2019**, *58*, 5126
$[Cd_3In_{17}Se_{31}Cl_4]^{9-}$	T4	Twisted Hexagonal *Dia*	67.1	DMSO	
$[Zn_4In_{16}S_{35}]^{14-}$ (ISC-16-Zn)	T4	*SOD*	74.4	Water/Acetone/DMF/, H_2O/EtOH(1:1)/Piperidine	*Inorg. Chem* **2020**,DOI:10.1021/acs.inorgchem.0c00621
$[Cd_{13}In_{22}S_{52}(1\text{-}MIM)_4]^{12-}$ (ISC-9)	T5	Cubic *Dia*	60.2	DMSO	*J. Am. Chem. Soc.* **2012**, *134*, 3619
$[Cu_5In_{30}S_{56}H_4]^{13-}$	T5	Cubic *Dia*	56.9	DMF/DMSO/CH_3CN +LiBr (0.2 M)	*J. Mater. Chem. A*, **2017**, *5*, 8519
$[Cd_6In_{28}S_{56}H_4]^{13-}$ (ISC-10-CdInS)	T5	Cubic *Dia*	56.9	DMF +LiBr (0.1 M) 0.1 M Na_2S	*Angew. Chem. Int. Ed.* **2018**,57, 5374 *Dalton Trans.*, **2018**,*47*, 6177.
$[Cu_8Ga_{17.5}Sn_{9.5}S_{56}]^{13.5-}$ (ISC-21)	T5	*BCU*	64.0	DMSO	*Adv. Mater. Interfaces* **2020**, *7*, 2000016
$[Zn_4Ge_4S_{13}O_4H_4]^{6-}$	P1	*PCU*	33.3	H_2O/EtOH (4:1)	*ACS Appl. Mater. Interfaces* **2018**, *10*, 13413
$[Cu_{5.88}In_{11.9}Sn_{8.22}S_{44}]^{13.54-}$	P2	Twisted *PCU*	60.7	H_2O/Acetone (1:1)	*Nano Res*, **2020**, DOI:10.1007/s12274-020-2936-0.
$[Cu_{6.09}Ga_{9.4}Sn_{10.51}S_{44}]^{11.67-}$	P2	Twisted *PCU*	60.3	H_2O/Acetone (1:1)	

[a] The formula of cations and solvent molecules are omitted for simplicity. The abbreviations of organic molecules including the formulas are listed as follows: CPA—Cyclopentylamine; dach—1,2-diaminocyclohexane; DBN—1,5-diazabicyclo [4.3.0] non-5-ene; 1-MIM—1-methylimidazole.

[b] T*n* (n=2, 3, 4, 5) and P*n* (n=1, 2) clusters referred to supertetrahedral clusters according to literatures.

[c] The intercluster packing pattern is obtained by treating each barycenter of the discrete cluster in compounds as a pseudo atom (X) and then connecting nearest adjacent X atom (at least four nearest adjacent X atoms are connected) to figure out the topological type of the arrangement mode. The abbreviations of topological symbols are described as follows: *BCU*—body centered cubic; *PCU*—primitive cubic; *Dia*—diamond; *MTN*—one zeolite framework type; *SOD*—sodalite-net.

[d] The solvent-accessible void space is calculated by the *PLANTON* program without taking all inorganic and/or organic cations and solvent molecules into account.

[e] NA means not mentioned in the article.

[f] As the compound is comprised of triangular ring-shaped $[Mn_9In_{33}Se_{60}(dach)_{24}]^{3-}$ anions and wheel-shaped $[In_{18}Se_{30}(dach)_6]^{6-}$ anions in a 2:1 ratio, the three discrete clusters are regarded as three different pseudo atoms and each pseudo atom connected only with the same type.

Table S6. Comparison of selected recent reported cluster-based crystalline metal chalcogenides for photocatalytic dye degradation.

Formula of metal chalcogenide anion [a]	Light source	Dye [b] (×10^{-5} M)	Catalyst (mg/mL)	Completion time (min)	Ratio (%)	*K*a (min^{-1})	Ref.
$[Ga_{16.1}In_{7.9}S_{40}(CPA)_8]^{8-}$	**350 W Xe lamp**	**MB, 3.5**	**0.25**	**5**	**98.1**	**0.8144**	**This work**
$[Ga_{24}S_{40}(CPA)_8]^{8-}$				**13**	**92.8**	**0.2000**	
$[Zn_4In_{16}S_{35}]^{14-}$	350 W Xe lamp	RhB, 10	0.5	20	90.5	NA [c]	*Inorg. Chem* **2020**,DOI:10.1021/acs.inorgchem.0c00621
$[Cu_5Sn_4GaSe_{14}]^{4-}$	350 W Xe lamp	MB, 1.8	0.5	40	98	0.0917	*Inorg. Chem.* **2020**, *59*, 7919
$[Cu_5In_{30}Se_{48.5}S_{3.5}Cl_3(Im)]^{12-}$	300 W Xe lamp, Visible light	CV, 2	0.67	80	99	NA	*Chem. Eur. J.* **2020**, *26*, 1624
$[Cd_6Ag_4(SPh)_{16}(DMF)(H_2O)(bpe)]_n$	300 W Xe lamp, λ > 420 nm	RhB, 4.18	1.25	20	98	NA	*Inorg. Chem.* **2020**,*59*,2121.
$[Sn_{20}O_{10}S_{32}]^{4-}$	300 W Xe lamp, Visible light	RhB, 20.2, pH=1	0.6	270	>98	NA	*Chem. Commun.*, **2019**, *55*, 11083
$Cd_6Ag_4(SPh)_{16}(tmdp)_2$	50 W Xe lamp, λ > 380 nm	RhB, 4.18	2	30	98	NA	*Dalton Trans.*, **2019**, *48*, 5505
$[Zn_4In_{14}Sn_2Se_{35}]^{12-}$	300 W Xe lamp, visible light	RhB, 1	0.5	360	98.3	0.01	*Inorg. Chem.* **2019**, *58*, 12011
		MB, 1		10	99.9	0.66	
$[In_{10}S_{12}Se_8]^{10-}$	300 W Xe lamp, visible light	RhB, 1	0.5	840	98.1	0.005	*Cryst.Growth Des.***2019**,*19*,5716
		MB, 1		16	99.9	0.309	
$[In_{8.75}Sn_{1.25}S_{18.5}]^{5.75-}$	300 W Xe lamp	MB, 12.5	0.1	80	90	NA	*Cryst.Growth Des.***2019**,*19*,4151
$[In_{10}S_4Se_{14}]^{6-}$	300 W Xe lamp, λ > 400 nm	MB, 1	0.2	20	98.6	0.197	*Inorg.Chem.Commum***2019**,*102*,251
		AcidicMO, 1, pH=2		25	98.2	0.169	
$[In_{10}S_{16}Cl_3(Bim)]^{5-}$	300 W Xe lamp, UV light	MO, 1	0.3	80	95.4	NA	*Cryst.Growth Des.***2018**,*18*,962
$[In_{10}Se_{13.8}Te_{2.2}Cl_3(Bim)]^{5-}$	300 W Xe lamp, Visible light			200	~ 97		
$[Mn_4Sn_6S_{20}]^{8-}$	275 W Hg lamp	CV, 1	0.75	150	91.7	NA	*Inorg.Chem,Commum.***2018**,*93*,73
$[Zn_{0.76}Ga_{0.70}Ge_{2.54}S_8]^{2.22-}$	300 W Xe lamp, visible light	RhB, 2.09	0.5	90	>98	0.03983	*Chem.Eur.J.* **2017**, *23*,11913.
$[In_{36}Se_{69}]^{30-}$	300 W Xe lamp	RhB, 8	0.5	240	>93	NA	*Inorg. Chem.* **2017**, *56*, 14763.
$[In_{42.6}Sn_{7.4}S_{90}]^{22.6-}$	300 W Hg lamp, visible light	MB, 10	0.5	60	95	0.05	*Cryst. Growth Des.***2017**,*17*,2936
$[Ag_5Sn_4Se_{12}]^{3-}$	300 W Xe lamp, λ > 420 nm	CV, 1	0.6	10	96	NA	*Cryst. Growth Des.***2017**,*17*,1235
$[AgSb_4S_7]^-$	300 W Xe lamp λ > 420 nm	RhB, 2.09	1.25	600	91	NA	*Inorg. Chem. Front.*,**2017**,*4*,954
$[AgSb_2S_4]^-$		CV, 2.45		5	94		

$[Ag_4Sn_3S_8]^{2-}$	300 W Xe lamp λ > 420 nm	CV, 1	0.6	200	92	NA	*Inorg. Chem.* **2016**, *55,* 10855.
$\{[Mn(2,2\text{-bipy})]_2As_2S_8\}^{2-}$	50 W Xe lamp λ > 400 nm	CV, 1	1	50	~100	NA	*J.SolidStateChem.* **2016**,*135*,183.
$[In_8Sn_8Se_{30}\ (Se_4)_2]^{2-}$	50 W Xe lamp, Visible light	MO, 1, pH=3	0.25	15	~ 100	NA	*Inorg. Chem.* **2015**, *54*, 5874.
$[Cu_{32}Sn_{12}S_{48}]^{16-}$	visible light	MB, 3.13	1	180	100	NA	*Inorg. Chem.* **2015**, *54*, 5301
$[Ge_{10}Sb_{28}S_{72}]^{20-}$	300 W Xe lamp, λ > 420 nm	RhB, 1	0.56	120	~94	NA	*Inorg. Chem.* **2015**, *54,* 8474.
$\{Mn_2Ga_4Sn_4S_{20}$ $[Mn_2(en)_5]_2\}$	500 W Xe lamp, Visible light	CV, 2.45	0.5	90	100	NA	*Dalton Trans.* **2015**, *44*, 2416.
$[Cd_8S(SPh)_{14}(DMF)(bpy)]_n$	250 W Xe lamp	RhB, 4.18 MB, 4.18	2	180	95	NA	*Dalton Trans.,* **2015**, *44*, 6400
$[Cd_6Ag_4(SPh)_{16}](bpe)_2$	500 W Xe lamp	RhB, 4.18	2	90	95	NA	*Chem. Commun.,* **2014**, *50*, 3710
1D and 2D $[HgSb_2S_5]^{2-}$	500 W Xe lamp, λ > 400 nm	RhB, 2.09	0.3	180	92	NA	*Cryst. Growth Des.***2014**,*14*,2411
$[GeSb_2S_6]^{2-}$	Xe lamp, λ = 400~780 nm	RhB, 1	0.3	480	85.1	NA	*CrystEngComm,* **2013**, *15*, 5007.
$[In_3Te_5(dien)]^-$	UV lamp, λ =375 nm	MO, 1.53	0.15	420	~ 98	NA	*CrystEngComm*, **2013**, *15*, 1194.
$[In_5Te_9(en)]^{3-}$	UV light	MO, 1.53	0.15	300	95.7	NA	*Inorg.Chem,Commum.***2013**,28,55.
$[In_2Sb_2Se_7]^{2-}$	4 W UV lamps, λ =254 nm	MO, 3.06	0.6	200	~ 100	NA	*CrystEngComm,* **2012**, *14*, 90
$[Mn(tren)]HgSb_2Se_5$	300 W Xe lamp, λ > 400 nm	RhB, 1	0.3	240	97	NA	*Dalton Trans.,* **2012**, *41,* 6689.

[a] The formula of cations and solvent molecules are omitted for simplicity. The abbreviations of organic molecules including the formulas are listed as follows: CPA—Cyclopentylamine; Im—Imidazole; SPh—Thiophenol; DMF—N,N-dimethylformamide; bpe—*trans*-1,2-bis(4-pyridyl)ethylene; tmdp—4,4′-trimethylenedipiperidine; Bim—1-butyl-2-methylimidazole; 2,2-bipy—2,2'-dipyridyl; en—Ethylenediamine; bpy—4,4′-bipyridine; dien—diethylenetriamine; tren—tris(2-aminoethyl)amine.

[b] The abbreviations of dye molecules are listed as follows: MB—Methylene blue; RhB—Rhodamine B; CV—Crystal Violet; MO—Methyl Orange.

[c] NA means not mentioned in the article.

References

1 Y. Wang, Z. Zhu, Z. Sun, Q. Hu, J. Li, J. Jiang and X. Huang, Discrete Supertetrahedral T5 Selenide Clusters and Their Se/S Solid Solutions: Ionic-Liquid-Assisted Precursor Route Syntheses and Photocatalytic Properties, *Chem. -Eur. J.*, 2020, **26**, 1624-1632.

2 M. Hao, Q. Hu, Y. Zhang, M. Luo, Y. Wang, B. Hu, J. Li and X. Huang, Soluble Supertetrahedral Chalcogenido T4 Clusters: High Stability and Enhanced Hydrogen Evolution Activities, *Inorg. Chem.*, 2019, **58**, 5126-5133.

3 C. Xue, L. Zhang, X. Wang, D. Hu, X.-L. Wang, J. Zhang, R. Zhou, D.-S. Li, H. Su and T. Wu, Enhanced Water Dispersibility of Discrete Chalcogenide Nanoclusters with a Sodalite-Net Loose-Packing Pattern in a Crystal Lattice, *Inorg. Chem.*, 2020, **59**, 15587-15594.